Long-term Doppler imaging of the star XX Trianguli indicates chaotic nonperiodic dynamo

K. G. Strassmeier, Zs. Kővári, M. Weber, T. Granzer

November 4, 2024

Supplementary Methods

STELLA robotic telescopes. The STELLA (short for STELLar Activity) Observatory[1] is located at the Izana ridge of the Teide Observatory on the Canary Island Tenerife (16°30'35"W, 28°18'00"N, at an altitude of 2390 m above sea level). No personnel is on site. STELLA consists of two independent 1.2m robotic telescopes, each of them serving a single dedicated instrument to avoid instrument changes. Both telescopes were manufactured by Halfmann Telescopes in Augsburg, Germany and are modern az-alt telescopes with a high slewing speed of 10°/s. The observatory housing consists of two roll-off roof-halves. So far, the building automation has never failed to protect the instruments during harsh weather phases. All of the algorithms developed in the beginning are still in place more-or-less unchanged, the only addition to the meteorological system has been the addition of a dust meter to allow the detection of low-altitude Sahara dust, a rather common phenomenon on the Canaries known as Calima.

The STELLA-I telescope is a f/8 Cassegrain system with two Nasmyth ports, one with a fixed mechanical flange and one with an image de-rotator. This telescope is optimized for wide field-imaging with a field-of-view of 24 arc minutes, but was originally fiber feeding the STELLA Echelle Spectrograph SES, which achieved first light on this telescope in September 2005. An acquisition and guiding unit was constructed for the fixed Nasmyth port, which held the fiber input to the spectrograph, a focus pyramid and a gray beam-splitter that diverted 4% of the light to a small CCD detector system.

The STELLA-II telescope is a spherical f/8.4 system laid out for only the prime focus at the top ring, where a refracting 5-lens corrector system corrects the light from the spherical primary mirror for a field of approximately one arc minute. An acquisition and guiding unit with a set of fixed atmospheric dispersion correctors, a focussing mechanism, and a CCD camera for guiding on the residual light reflected from an inclined pinhole mask, feeds the light into a fiber for SES.

The formal inauguration of the observatory took place in May 2006. SES science was started soon thereafter, including the target in this paper. The second instrument, a wide-field imaging photometer named WiFSIP (Wide Field STELLA Imaging Photometer) was completed in 2009 and delivered to Tenerife in 2010, where it was mounted on STELLA-I. At the same time, the SES input fiber was moved to STELLA-II achieving its second "first light" in May 2010.

STELLA Echelle Spectrograph (SES). SES is a fiber-fed fixed-format echelle spectrograph. Its white-pupil design with an R2 grating provides a resolving power of 55 000 over a wavelength range of 390–880 nm with a sampling of three pixels per resolution element. At a wavelength of 600 nm this corresponds to an effective resolution of 5.5 km s^{-1} or 110 mÅ. The average dispersion is 45 mÅ/pixel. Its current detector is an e2v 4k$\times$4k CCD with 15 μm pixels. The effective spectral resolution is made possible with a 2-slice image slicer and a 67-μm (octagonal) fiber with a projected sky aperture of 3.8 arc seconds. The spectrograph is placed in a thermal housing but not in a pressure sealed environment, its radial velocity (RV) stability is thus limited to 30 m s^{-1} for an ideal target. Further details and references on the performance of the system can be found in previous applications to similar giant stars.[2]

SES spectra are automatically reduced using the IRAF-based STELLA data-reduction pipeline SESDR.[3] Wavelength calibration is based on Th-Ar cathode-lamp spectra. SESDR makes sure that only identical lines are included in the wavelength solution over time because spurious emission lines may pop up during the aging of the lamp. All CCD images were corrected for bad pixels and cosmic-ray impacts. Bias levels were removed by subtracting the average overscan from each image followed by the subtraction of the mean of the (already overscan subtracted) master bias frame. The target spectra were flattened by dividing by a master flat which has been normalized to unity. Nightly master flats are constructed from around 100 individual flats observed during dusk and dawn. Fifty such nightly flats are then used to create the master flat itself. After removal of scattered light, the one-dimensional spectra were extracted using an optimal-extraction algorithm. The blaze function was then removed from the target spectra, followed by a wavelength calibration using consecutively recorded Th-Ar spectra. Finally, the extracted spectral orders were continuum normalized by dividing with a flux-normalized synthetic spectrum of comparable spectral classification as the target.

Wolfgang and Amadeus Automatic Photoelectric Telescopes (APT). The APTs used for the XX-Tri photometry were the two automated Wolfgang (T6) and Amadeus (T7) 0.75 m twin telescopes[4,5] located at Fairborn Observatory in southern Arizona. Both telescopes are simple flux collectors with a Cassegrain f/2 primary mirror and f/8 overall focal ratio and equipped with a single-channel photometer with a photoelectric multiplier as the scientific detector. The Amadeus photometer used an EMI-9828 S-20/B multialkali cathode and a prismatic window which gives good red response and was optimized for Johnson BVR. The Wolfgang photometer used a bi-alcali EMI-9124/QB tube for blue sensitivity and was optimized for Strömgren $uvby$. A respective flip mirror diverts the light path after the diaphragm to an integrating fast-scan CCD camera which is used to acquire and center the object to be measured. The inside of the photometer housings is pressurized by an air dryer and cooled by a water circuit. The Wolfgang system was available for XX Tri only in the early years from 1997–2009. The photometric performance of Amadeus faded over the past ten years. After an exchange of the EMI-9828 S20 tube with a blue-sensitive ET-9124B tube in 2018 (at JD 2,458,132; Jan. 13, 2018) the system briefly performed better but again faded soon thereafter. In January 2019, we decided to retire the telescope.

Supplementary Figures

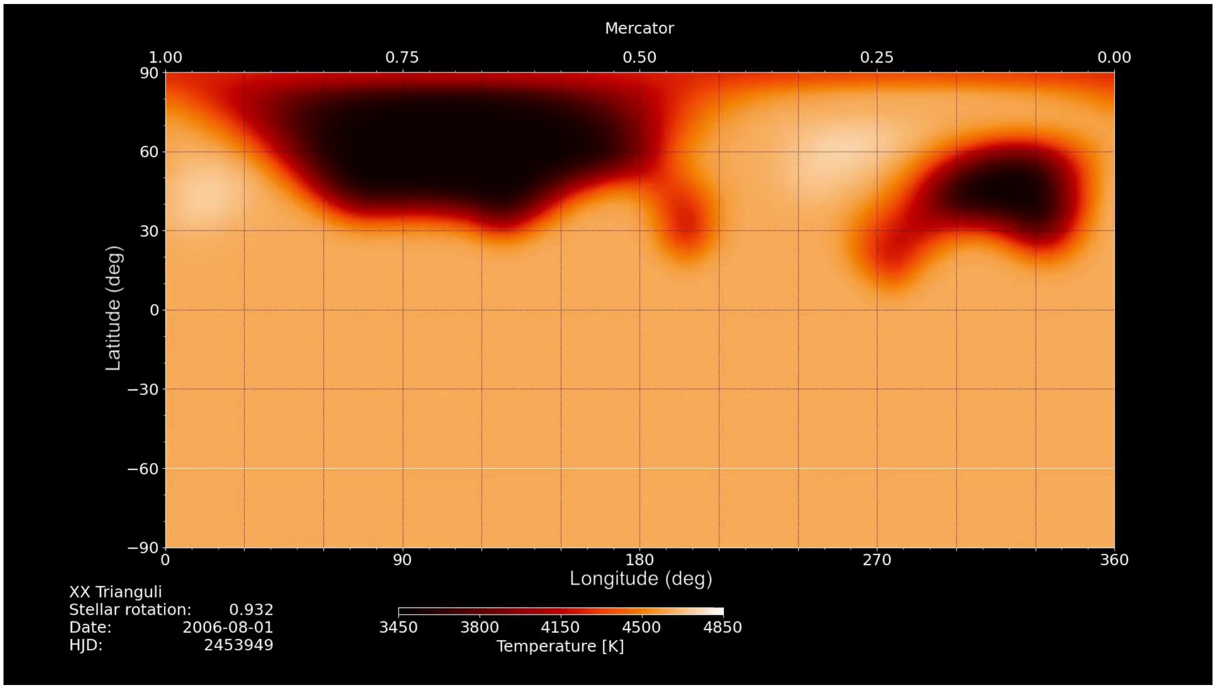

Supplementary Figure 1: Screen snapshot from Supplementary Movie 2. Starspot evolution on XX Tri for 16 years in equidistant Mercator projection. Latitude is plotted versus Longitude in degrees. The surface grid is spaced in 30-degree steps. The white line at latitude $-60°$ indicates the surface-visibility limit due to the projected inclination of the stellar rotation axis. The bottom left insert indicates the time. Time is counted in stellar rotations, in civil date, and in heliocentric Julian date (HJD). The real-time coverage is 237 stellar rotations from August 2006 to February 2022, or 5670 days. Surface color is coded in terms of temperature as defined in the color bar. Movie format is mp4. Movie duration is three minutes and nine seconds.

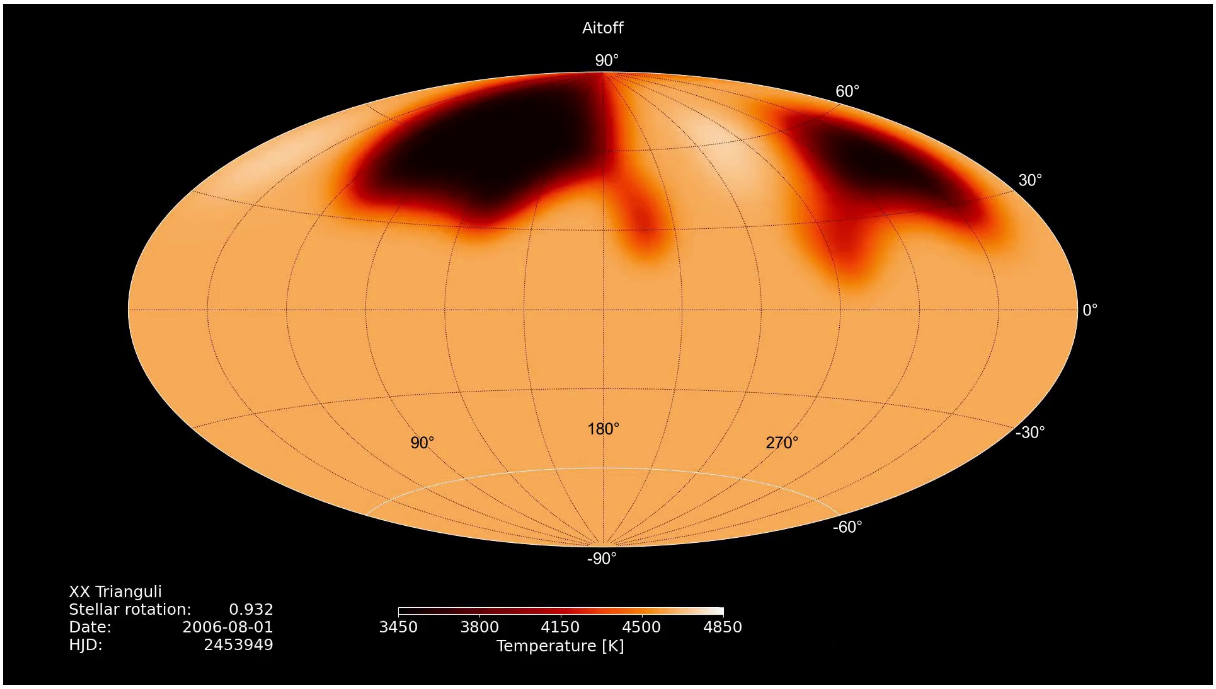

Supplementary Figure 2: Screen snapshot from Supplementary Movie 3. Starspot evolution on XX Tri for 16 years in true-area Aitoff projection. Latitude is plotted versus Longitude in degrees. The surface grid is spaced in 30-degree steps. The white line at latitude $-60°$ indicates the surface-visibility limit due to the projected inclination of the stellar rotation axis. The bottom left insert indicates the time. Time is counted in stellar rotations, in civil date, and in heliocentric Julian date (HJD). The real-time coverage is 237 stellar rotations from August 2006 to February 2022, or 5670 days. Surface color is coded in terms of temperature as defined in the color bar. Movie format is mp4. Movie duration is three minutes and nine seconds.

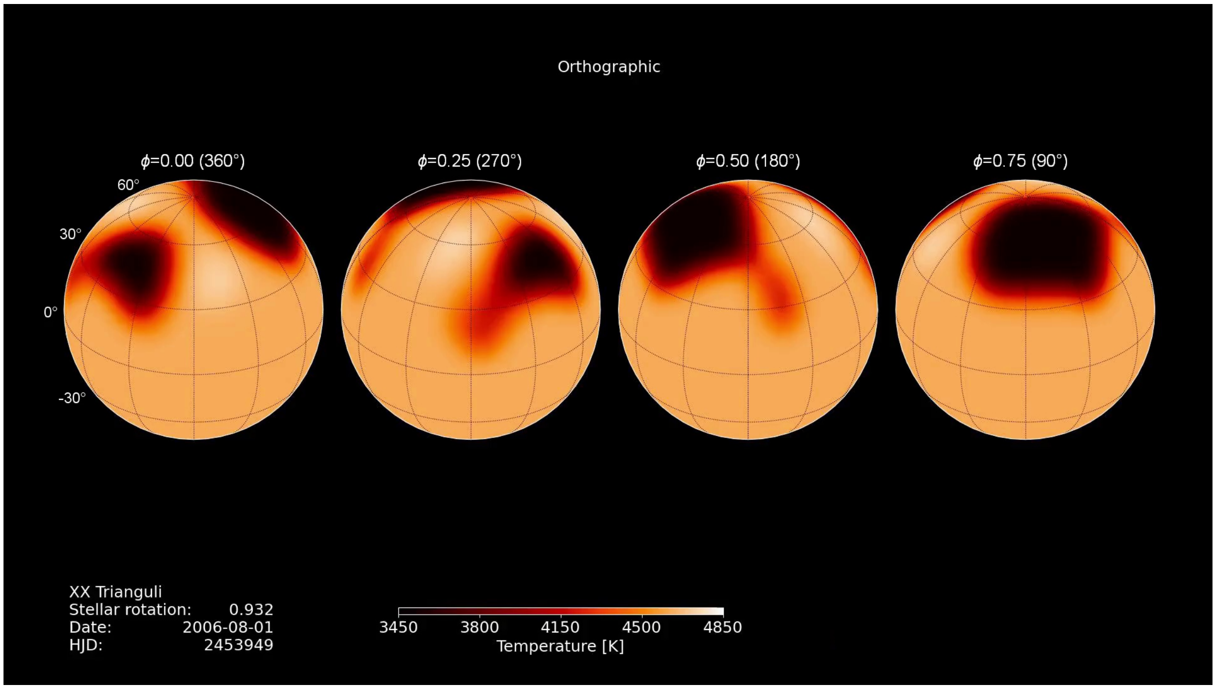

Supplementary Figure 3: Screen snapshot from Supplementary Movie 4. Starspot evolution on XX Tri for 16 years in orthographic projection at four equidistant rotational phases. Latitude is plotted versus Longitude in degrees. The surface grid is spaced in 30-degree steps. The longitude of the central meridian is identified as its rotational phase at the top of each image projection (0.00, 0.25, 0.50, and 0.75). The white line at latitude -60° indicates the surface-visibility limit due to the projected inclination of the stellar rotation axis. The bottom left insert indicates the time. Time is counted in stellar rotations, in civil date, and in heliocentric Julian date (HJD). The real-time coverage is 237 stellar rotations from August 2006 to February 2022, or 5670 days. Surface color is coded in terms of temperature as defined in the color bar. Movie format is mp4. Movie duration is three minutes and nine seconds.

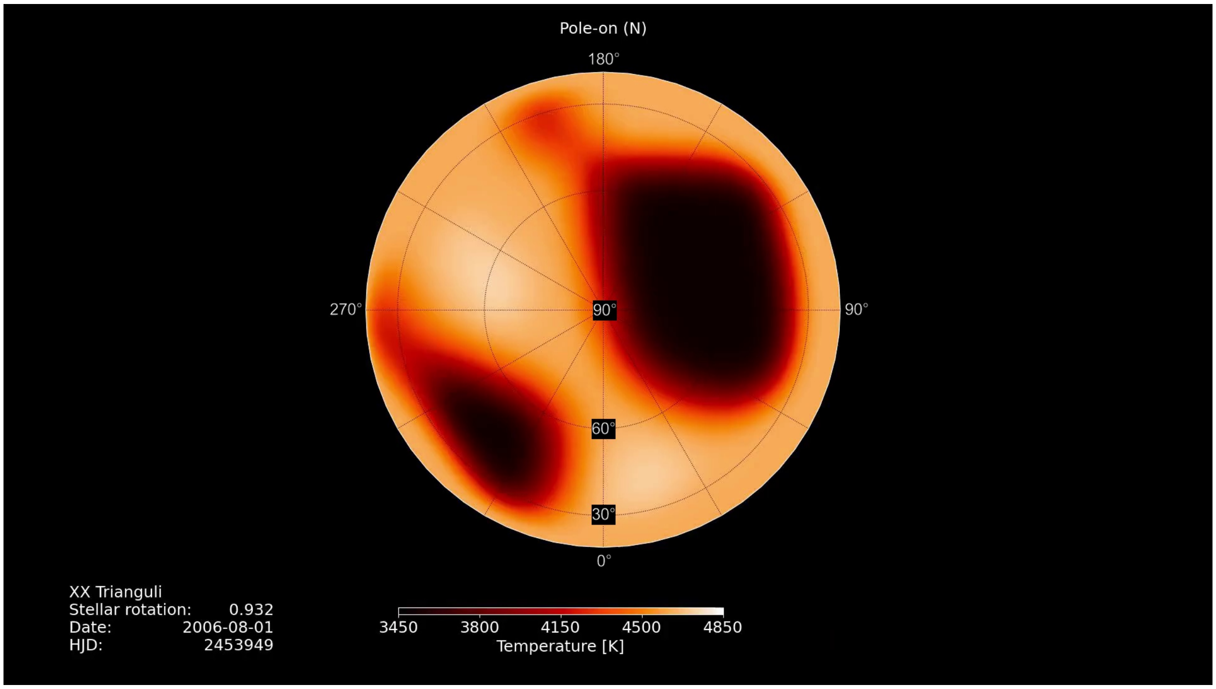

Supplementary Figure 4: Screen snapshot from Supplementary Movie 5. Starspot evolution on XX Tri for 16 years in a meshed pole-on projection. Latitude is plotted versus Longitude in degrees. The surface grid is spaced in 30-degree steps. The round image circumference represents the stellar equator at a latitude zero. No surface regions below the equator are visible. The plot emphasizes the one visible rotational pole of the star. The bottom left insert indicates the time. Time is counted in stellar rotations, in civil date, and in heliocentric Julian date (HJD). The real-time coverage is 237 stellar rotations from August 2006 to February 2022, or 5670 days. Surface color is coded in terms of temperature as defined in the color bar. Movie format is mp4. Movie duration is three minutes and nine seconds.

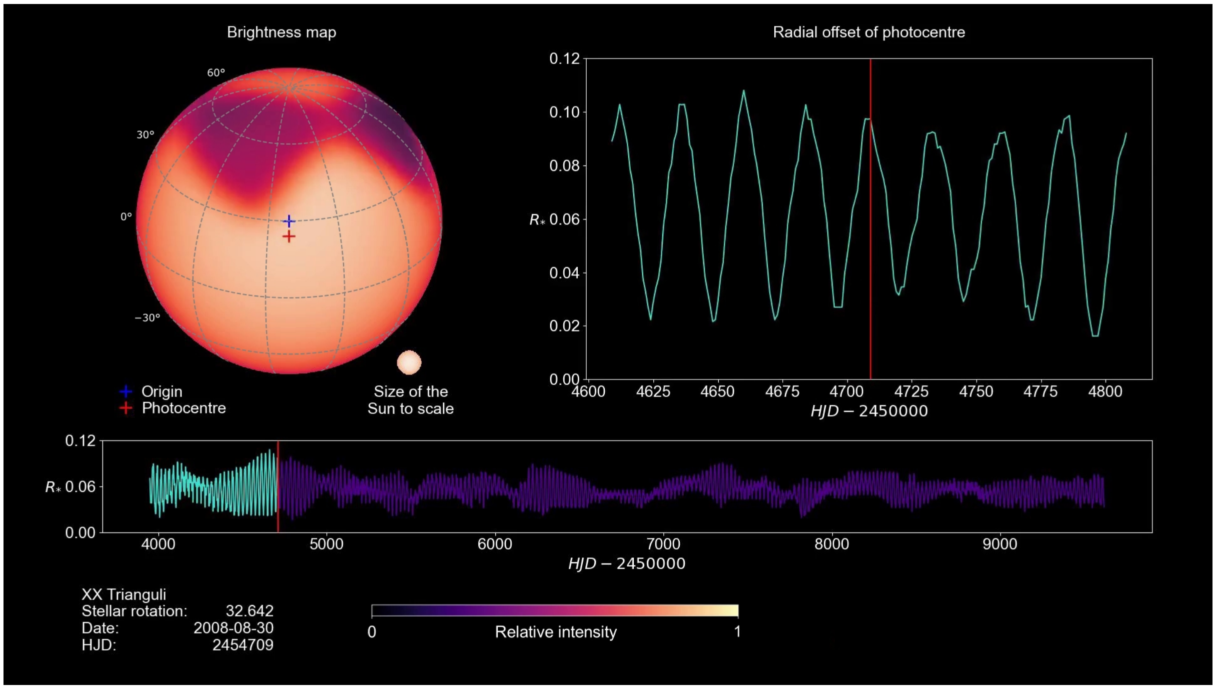

Supplementary Figure 5: Screen snapshot from Supplementary Movie 6. Brightness surface in orthographic projection with dynamic graphics for the stellar-disk radial photocenter offsets. This movie version represents the radial photocenter offsets as measured directly from the Doppler images. The two disk pluses represent the original geometric disk center (blue colored plus) and the photometric disk center (red colored plus), respectively. The relative size of the solar disk is indicated for comparison. The top right panel plots the radial photocenter offset $R_{\star}$ in units of the projected stellar disk radius (=1) versus time in heliocentric Julian dates for a time window of 100 days. The vertical cursor relates to the current phase of the orthographic brightness movie on the left. The full 16-year time coverage is shown in the lower panel. The bottom left insert indicates the overall time. Time is counted in stellar rotations, in civil date, and in heliocentric Julian date (HJD).

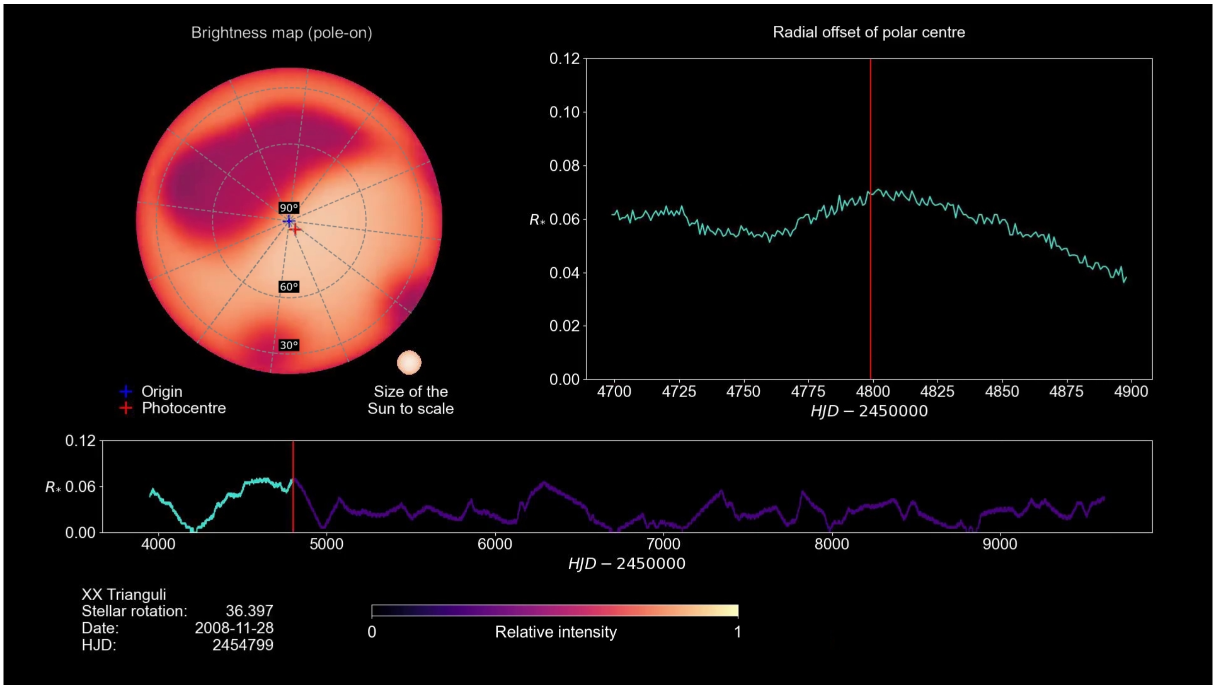

Supplementary Figure 6: Screen snapshot from Supplementary Movie 7. Brightness surface in pole-on projection and dynamical graphics for the stellar-disk radial photocenter offsets. This movie version shows the same radial photocenter offsets as in Movie 6 but projected as if XX Tri were seen pole-on. The pole-on projection emphasizes eventual long-term photocenter changes due to a (polar) magnetic cycle. No periodic variations are detected though. The two pluses represent the original disk center, now identical with the one visible rotational pole (blue colored plus), and the projected photometric disk center (red colored plus), respectively. The top right panel plots the radial photocenter offset $R_\star$ in units of the projected stellar disk radius (=1) versus time in heliocentric Julian dates for a time window of 100 days. The vertical cursor relates to the current phase of the pole-on projected brightness movie on the left. The full 16-year time coverage is shown in the lower panel. The bottom left insert indicates the overall time. Time is counted in stellar rotations, in civil date, and in heliocentric Julian date (HJD).

a

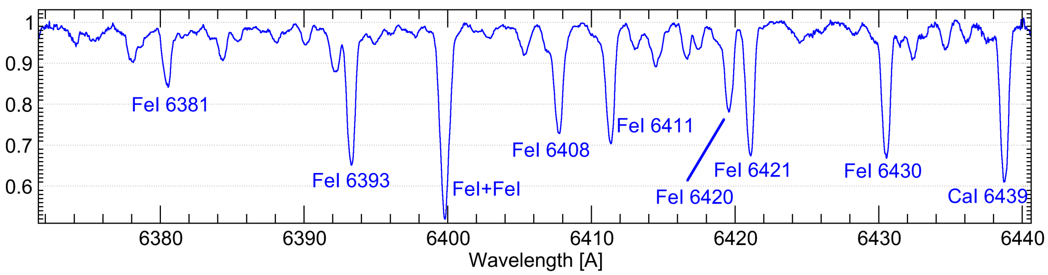

b

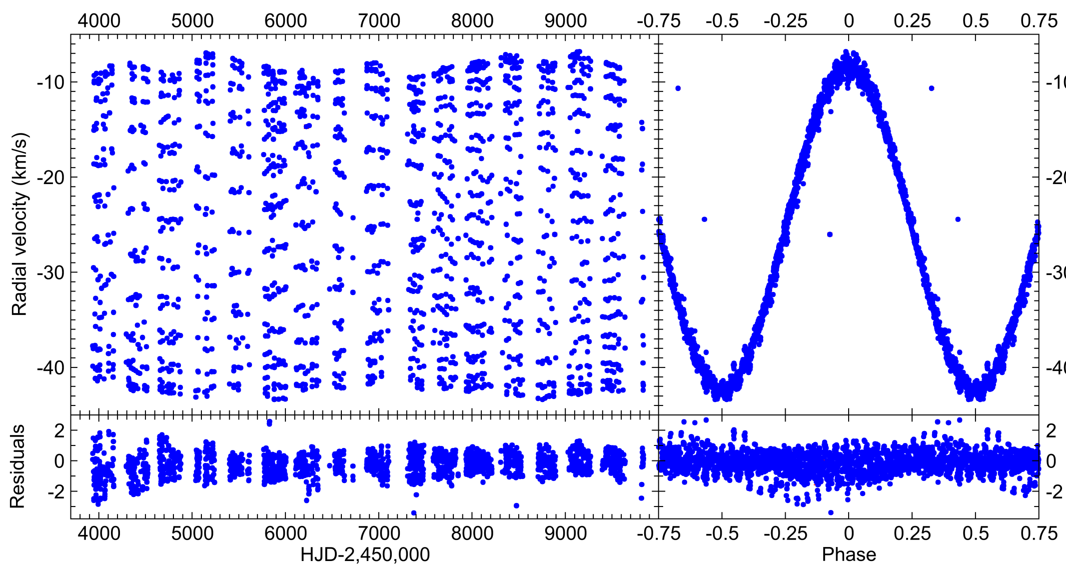

Supplementary Figure 7: Full STELLA SES data sample of XX Tri. a Example spectrum for an (arbitrary) wavelength range 6370–6440 Å. Intensity is normalized to the continuum in relative units, wavelength is in Angstroems. Most of the spectral lines in this wavelength range are neutral iron lines. Six of the lines (Fe I 6393, 6408, 6411, 6421, 6430, and Ca I 6439) marked in the plot are used for the Doppler imaging. **b** Radial velocities in km s^{-1} as a function of time; left two panels are versus Heliocentric Julian Date (HJD 2,450,000), right two panels are versus rotational phase. The respective lower panels are the residuals in km s^{-1} after removal of a preliminary orbital fit from the data. Source data are provided as a Source Data file.

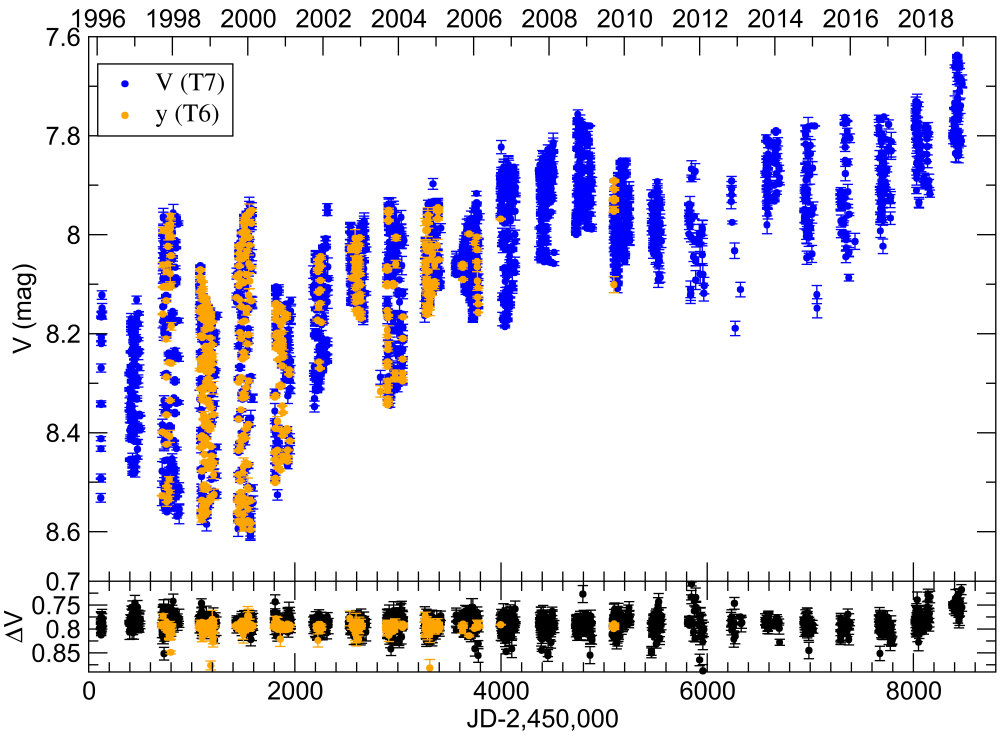

Supplementary Figure 8: Contemporaneous APT photometry of XX Tri. A maximum V brightness of 7.64 mag was reached in 2018/19. Amadeus (T7) data were taken in Johnson V (blue dots), Wolfgang (T6) data were taken in Strömgren y (green dots) and converted to Johnson V. The lower panel is the control light curve for the brightness difference of a comparison star minus a check star. Error bars denote the rms from three individual measures. Source data are provided as a Source Data file.

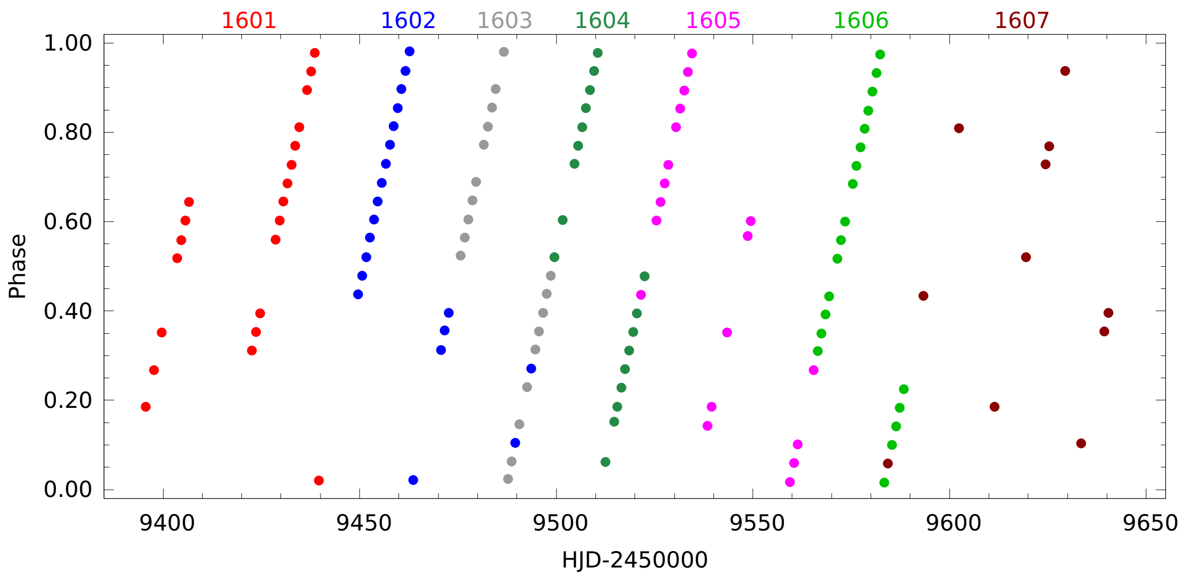

Supplementary Figure 9: Seasonal phase coverage for the observing season 2021/2022. Rotational phase is plotted versus Heliocentric Julian Date (HJD) in days. The colors of the symbols identify the spectra for the (seven) individual Doppler images in this season. There were no unused spectra in the season shown. Images are identified on the top with their map ID no. from Supplementary Data 1. Phase values and HJDs of the spectra used for each Doppler image are listed in Supplementary Data 2.

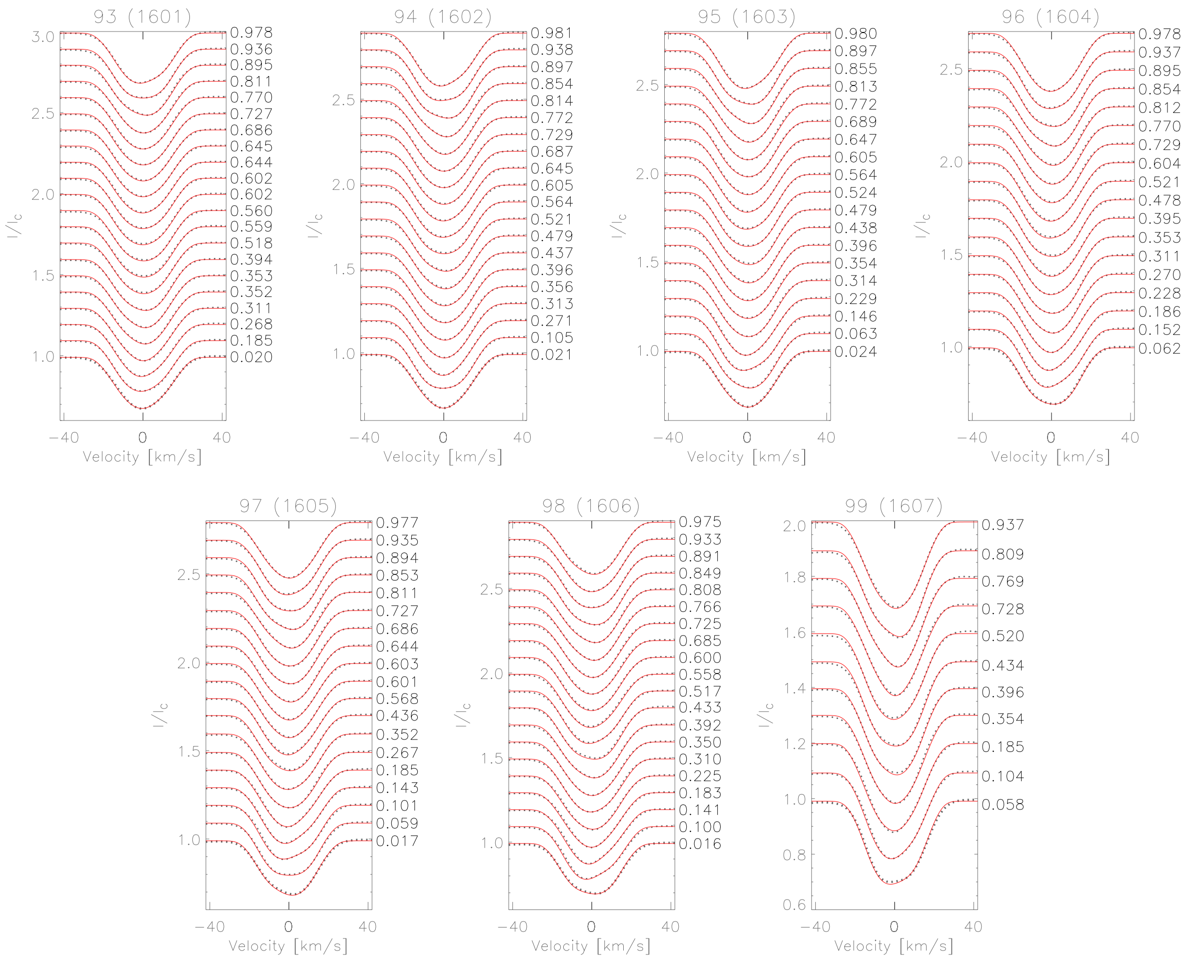

Supplementary Figure 10: Observed and inverted line profiles. Shown are only the data for observing season 2021/22. Each panel compares the observed (dotted lines) and inverted (solid lines) line profiles for one Doppler image. The image is identified from Supplementary Table 1 with its running number and the map ID no. on top of the panel. The respective rotational phases are listed on the side. Rotation advances always from bottom to the top. The data and the fits are provided in a source data file.

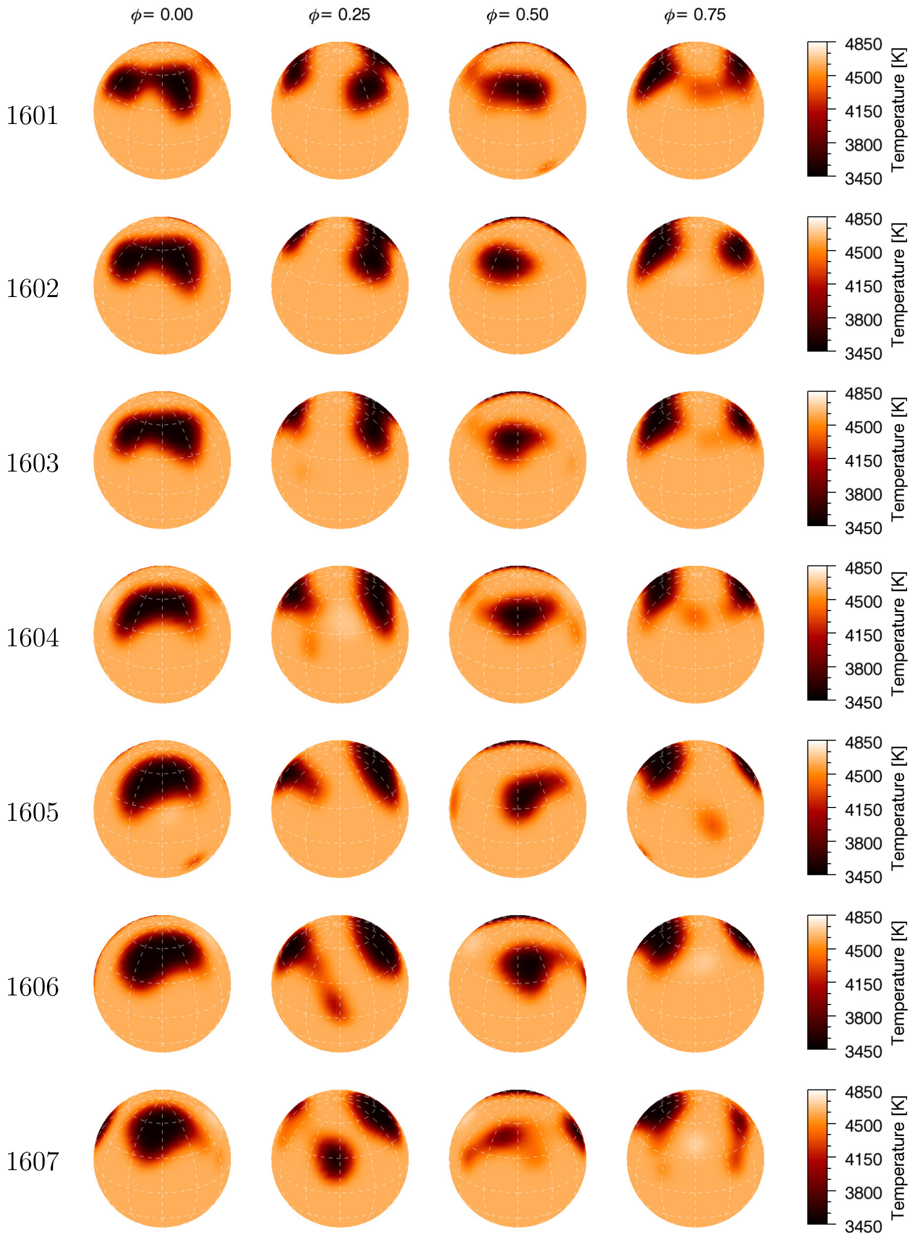

Supplementary Figure 11: Doppler images for the observing season 2021/2022. Shown are orthographic projections at four rotational phases ϕ separated by 90°, and for seven separate rotations. Surface latitude and longitude is indicated in steps of 30° in every map. Color being the surface temperature according to the scale on the right side. The unspotted photospheric temperature is 4630 K. Shown are images 1601 to 1607 according to the listing in Supplementary Data 1. Time increases from top to bottom.

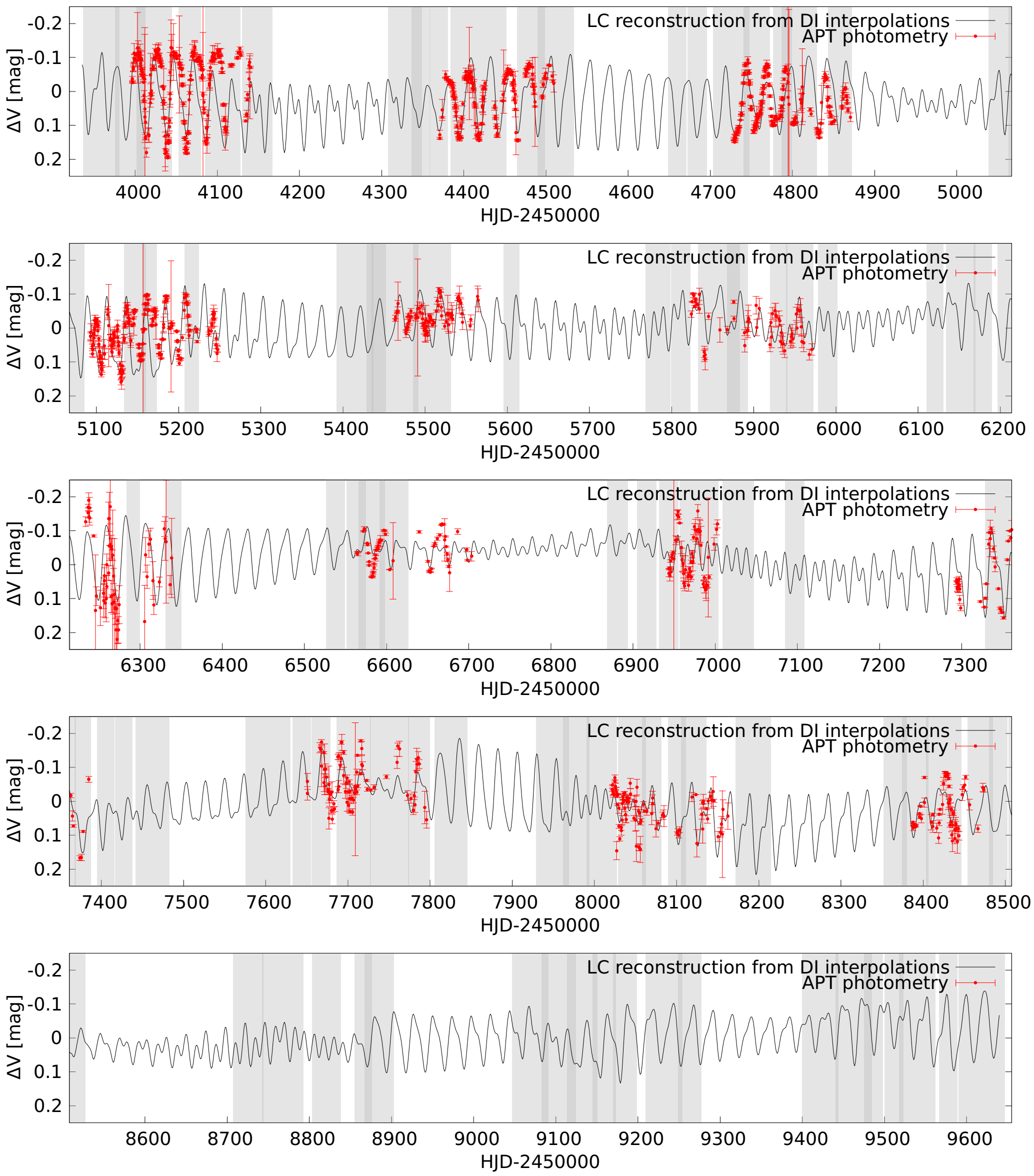

Supplementary Figure 12: Comparison of the APT-photometry with the Doppler-image predictions. The APT-data from Supplementary Fig. 8 (red dots with error bars defined as the rms from three individual measures) are compared with the predicted brightness variations calculated based on the brightness map presented in Supplementary Movie 6 (black line). The grey shaded areas indicate the times of our Doppler images. The APT data had to be de-trended in order to remove the long-term trend at least to first order. The comparison indicates principally a reasonable match but residual zero-point variations from one observing season to the next remain.

References

[1] Strassmeier, K. G. *et al.* The STELLA robotic observatory. *Astron. Nachr.* **325**, 527 (2004).

[2] Strassmeier, K. G., Weber, M., Granzer, T., & Järvinen, S. Rotation, activity, and lithium abundance in cool binary stars. *Astron. Nachr.* **333**, 663 (2012).

[3] Weber, M., Granzer, T., & Strassmeier, K. G. STELLA: 10 years of robotic observations on Tenerife. In Peck, A. B., Seaman, R. L. & Benn, HC. R. (eds.) *Observatory Operations: Strategies, Processes, and Systems VI*, vol. 9910 of *Society of Photo-Optical Instrumentation Engineers (SPIE) Conference Series*, 99100N (2016).

[4] Strassmeier, K. G., Boyd, L. J., Epand, D. H. & Granzer, T. Wolfgang-Amadeus: The University of Vienna twin automatic photoelectric telescope. *Publ. Astron. Soc. Pac.* **109**, 697 (1997).

[5] Strassmeier, K. G., Granzer, T., Boyd, L. J., & Epand, D. H. Wolfgang-Amadeus: The University of Vienna twin robotic photoelectric telescopes. *Proc. SPIE* **4011**, 157 (2000).